Spacecraft Environment Discharges in the Geostationary Environment

Radio Signatures and Relationship to Plasma Population and Geomagnetic Indices

Todd S. Anderson, Amitabh Nag, Erin H. Lay, Philip A. Fernandes, and Brian A. Larsen
Los Alamos National Laboratory

2026 Space Weather Workshop, April 27-May 1

Key Points

- The STPSat-6 geostationary satellite carries both a wideband radio frequency receiver instrument and a suite of electrostatic analyzers, enabling comparisons of electrostatic discharge signatures with plasma population for the first time since the SCATHA mission in the late 1970s.
- We investigate the timing relationship between discharge signature occurrence rate and enhanced particle flux and geomagnetic indices.
- Possible causes of discharge occurrence are considered, including plasma sheet injections, eclipse, and plasmasphere dynamics.

Instruments and data

STPSat-6, at -111.6°E in GEO, hosts the **Radio Frequency Sensor (RFS)** and **Z-Plasma Spectrometer (ZPS)**.

RFS (Lay et al., 2024):

- VHF software-defined radio with high (120-140 MHz) and low bands (35-55 MHz), two active crossed-dipole antennas.
- Mainly detects frequency-dispersed lightning discharges, e.g. TIPPs (Pailoor et al., 2025).
- Also detects non-dispersed transients, i.e. **spacecraft environment discharges (SEDs)**; typically high amplitude.

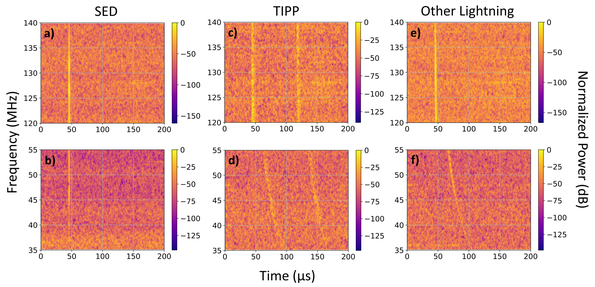

Figure 1: Examples of three different classes of RFS detections: (left) SEDs, (center) TIPPs, and (right) non-TIPP lightning. Adapted from Nag et al. (2025).

ZPS (MacDonald et al., 2009; Nag et al., 2025):

- Low-energy instrument ("ZPS Lo") is a top-hat electrostatic analyzer that measures electrons and positive ions (typically H+) in 72 differential energy channels between 2 eV/q and 50 keV/q.
- Full energy range of both electrons and ions measured every 110 s.

Dataset: March 1, 2022 through May 17, 2023.

- RFS count rates computed by summing detections in 1-minute bins.
- SEDs found in high-band events using an amplitude saturation flag.
- ZPS particle flux resampled at 1-minute cadence.
- Geomagnetic indices: Dst available at 1-hour cadence, Kp resampled from 3-hour to 1-hour cadence; SuperMAG SML, SMU, SMR and respective local time indices provided at 1-minute cadence.

SED event definition

SEDs are observed to occur in high-count-rate clusters that may last several tens of minutes or hours. We preprocess these clusters as follows:

1. Smooth the 1-minute count rate with 10-minute moving average.
2. Compute the envelope of the smoothed count rate.
3. Find envelope peaks, and peak start and end times based on envelope dropping below 5 counts/min preceding and following each peak.
4. SED events are peaks in this envelope with count rate $>$ 20 counts/min and duration $>$ 10 min.

See Figures 5a and 7a for examples. We identified 235 SED events in the dataset using this procedure.

Acknowledgements

This work was supported by the Defense Nuclear Nonproliferation Research and Development Office of the National Nuclear Security Administration and the Department of the Air Force. The experiment was integrated and flown by the DoD Space Test Program. Los Alamos National Laboratory is operated by Triad National Security, LLC, under contract number 89233218CNA000001. We sincerely appreciate the efforts of the RFS and ZPS instrument teams, including scientists, engineers, technicians, and support personnel. We gratefully acknowledge the GFZ Helmholtz Centre, the World Data Center for Geomagnetism at Kyoto, and the SuperMAG collaborators for providing the Kp, Dst and SuperMAG indices, respectively.

SEA: plasma flux and geomagnetic indices

We investigate the timing relationship between SED events, particle flux and geomagnetic indices using a superposed epoch analysis (SEA) technique, where SED event peaks are used as the time reference. SEA curves for SED count rate, electron flux and ion flux are shown in Figure 2. Particle flux SEA curves are normalized by dividing by (number of epochs $\times$ mean flux in channel).

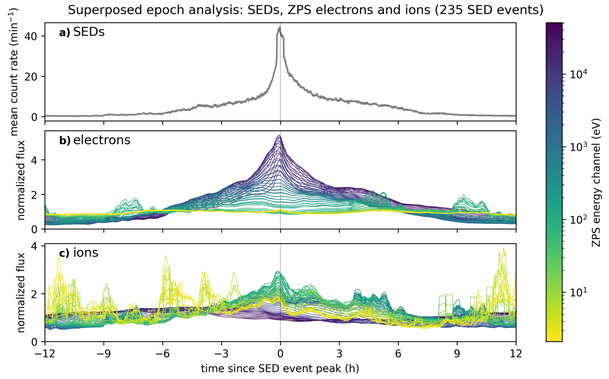

Figure 2: SEA of SED count rate (top), ZPS electron flux (middle) and ZPS ion flux (bottom).

The time offset and magnitude of the electron and ion SEA peaks from Figure 2b-c are shown in Figure 3. Relative to SED event peaks:

- Electrons in the 4-8 keV range peak around 8 minutes earlier.
- Ions in the 100 eV-1keV range peak around 5-7 minutes earlier.

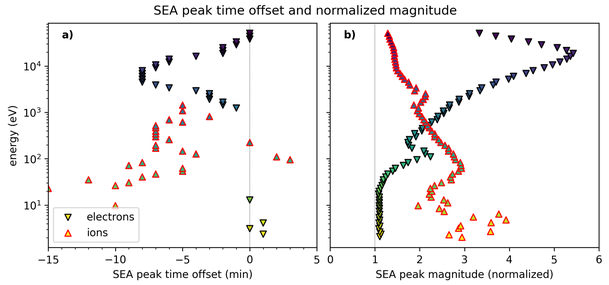

Figure 3: Peak time offset (left) and magnitude (right) from ZPS electron and ion flux curves in Figure 2b-c.

The SEA curves showing the mean response of Kp, Dst and SuperMAG geomagnetic indices during SED events are plotted in Figure 4.

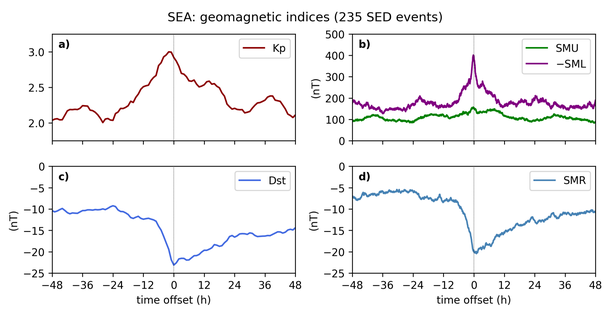

Figure 4: SEA of (a) Kp, (c) Dst and SuperMAG (b) auroral electrojet indices SMU, SML and (d) ring current index SMR.

- Background: (i) SEDs: 2 ± 1 min^{-1}; (ii) Kp: 2.0 ± 0.2; (iii) Dst: -10 ± 2 nT; (iv) SML: -190 ± 10 nT; (v) SMR -7 ± 2 nT.
- SEA peak (magnitude−background): (i) SEDs: 40 min^{-1}; (ii) Kp: 0.8; (iii) Dst: -11 nT; (iv) SML: -200 nT; (v) SMR -12 nT.
- Index median differences between SED event peaks and whole time series are similar to SEA peak prominences.

Local time dependence and eclipse signatures

Geostationary spacecraft often experience significant negative surface charging in eclipse. An example comparison of SED count rate, particle flux and SuperMAG auroral electrojet indices is shown in Figure 5.

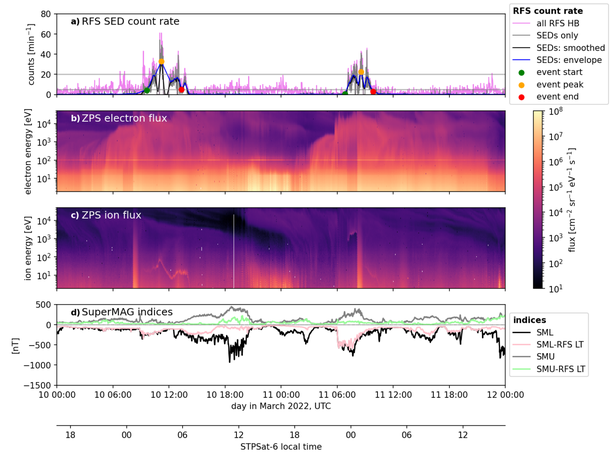

Figure 5: Case study of 2 days in March 2022 showing eclipse signatures in electron and ion flux.

We compute the local time averages of SED count rate and ZPS electron and ion flux. These averages are plotted in Figure 6, with the same normalization as in Figure 2.

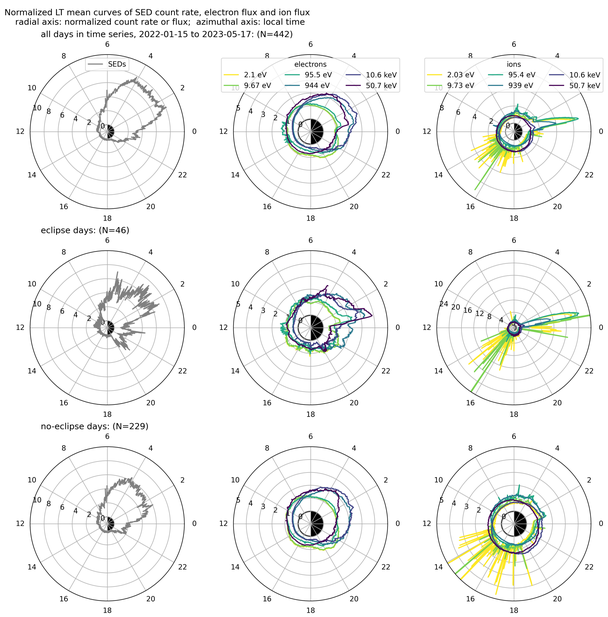

Figure 6: Local time mean of SED count rate (*left column*), electron flux (*center column*) and ion flux (*right column*) for all days in dataset (*top row*), satellite eclipse days (*middle row*) and days when the satellite was never in eclipse (*bottom row*).

- SEDs preferentially occur in the postmidnight through dawn (LT 0-6) sector. SCATHA also measured large frame potential and discharge events in this sector!
- Flux of 10-50 keV electrons is enhanced in this sector for all data subsets, consistent with gradient/curvature drift from plasma sheet injection at midnight/premidnight LT.
- Electron flux $<$1 keV is depleted during eclipse, and all ion energies (particularly $<$100 eV) are enhanced post-eclipse. Ion "pileup" signature is sometimes observed.
- *What is the cause of cold ion enhancements apparent in local afternoon?*

Substorm and plasmspheric influence

SED events are also observed during energy-coherent electron flux enhancements that may be linked to plasmapause or plasmaspheric drainage plume crossing. Example events are shown in Figure 7.

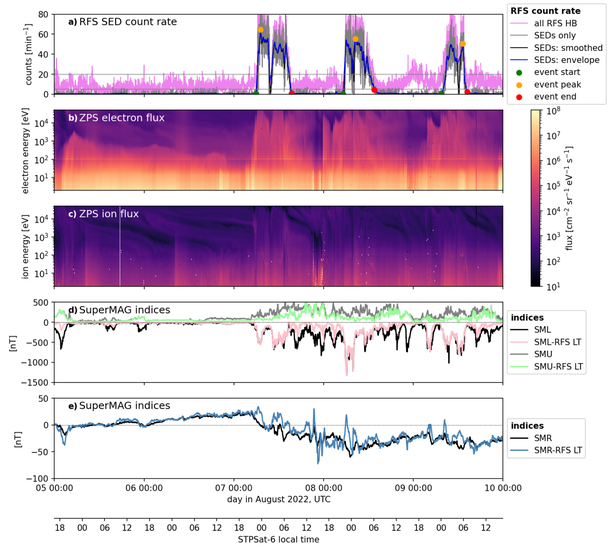

Figure 7: Case study of 5 days in August 2022 showing possible plasmasphere filling and drainage.

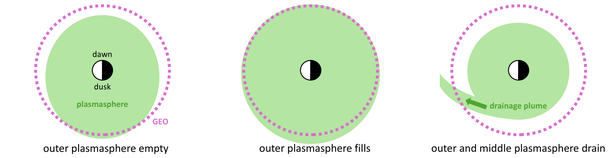

Figure 8: Schematic of plasmapause location relative to GEO for (a) normal geomagnetic activity, (b) a multi-day calm period, and (c) storm time. Adapted from Borovsky and Denton (2008).

Summary

- We compared collocated geostationary RF transient ("SED") and plasma flux measurements onboard a geostationary spacecraft.
- Using a superposed epoch analysis (SEA) technique, peak flux of 1-10 keV electrons and 0.1-1 keV ions was found to precede peak SED occurrence rate by 5-8 minutes.
- Kp, Dst and SuperMAG auroral electrojet and ring current indices were found to be more disturbed during SED event peaks.
- Local time and particle energy dependence of SED events suggest they are triggered by plasma sheet injections, but other causes are possible.
- Future work: develop metrics to forecast SED event onset and relate to spacecraft surface potential.

References

Borovsky, J. E., & Denton, M. H. (2008, September). A statistical look at plasmaspheric drainage plumes. *Journal of Geophysical Research: Space Physics*, *113*(A9). Retrieved 2026-02-03, from `https://agupubs.onlinelibrary.wiley.com/doi/full/10.1029/2007JA012994` doi: 10.1029/2007JA012994

Lay, E. H., Romero, L., Peterson, M., Nag, A., Behnke, S., & Pailoor, N. (2024). Radio Frequency Sensor: Very High Frequency Radio Frequency Lightning Detection in Geostationary Orbit. *Radio Science, 59*(6), e2023RS007931. doi: 10.1029/2023RS007931

MacDonald, E. A., Funsten, H. O., Dors, E. E., Thomsen, M. F., Janzen, P. H., Skoug, R. M., ... Reisenfeld, D. (2009). New Magnetospheric Ion Composition Measurement Techniques. *AIP Conference Proceedings*, *1144*(1), 168–172. doi: 10.1063/1.3169283

Nag, A., Lay, E. H., Larsen, B. A., Mark, M. D., Fernandes, P. A., & Attanasio, A. R. (2025). Radio Frequency Transients Correlated with Electron Flux Measured On-Board the STP-Sat6. *Advances in Space Research*. doi: 10.1016/j.asr.2025.07.026

Pailoor, N. A., Lay, E. H., Nag, A., & Anderson, T. S. (2025). Statistical Analysis of Transionospheric Pulse Pairs and Inferences on Their Characteristics. *Journal of Geophysical Research: Atmospheres*, *130*(15), e2025JD043403. doi: 10.1029/2025JD043403

Los Alamos NATIONAL LABORATORY
National Nuclear Security Administration
Managed by Triad National Security, LLC, for the U.S. Department of Energy's NNSA.
LA-UR-26-23222